Optik - International Journal for Light and Electron Optics 281 (2023) 170830

Contents lists available at ScienceDirect

Optik

journal homepage: www.elsevier.com/locate/ijleo

Investigating the influence of Eu-doping on the structural and optical characterization of cadmium oxide thin films

A.A.M. Farag [a,*], M.I. Mohammed [b], V. Ganesh [c], H. Elhosiny Ali [c,d], A.M. Aboraia [e,f], Yasmin Khairy [d], H.H. Hegazy [c], V. Butova [e], Alexander V. Soldatov [e], H. Algarni [c], H.Y. Zahran [c,g,h], I.S. Yahia [c,g,h,i]

[a] Thin Film Laboratory, Physics Department, Faculty of Education, Ain Shams University, Roxy, 11757 Cairo, Egypt
[b] Nanoscience Laboratory for Environmental and Bio-medical Applications (NLEBA), Metallurgical Lab. 1, Physics Department, Faculty of Education, Ain Shams University, Roxy, 11757 Cairo, Egypt
[c] Laboratory of Nano-Smart Materials for Science and Technology (LNSMST), Department of Physics, Faculty of Science, King Khalid University, P. O. Box 9004, Abha, Saudi Arabia
[d] Physics Department, Faculty of Science, Zagazig University, Zagazig 44519, Egypt
[e] The Smart Materials Research Institute, Southern Federal University, Sladkova 178/24, 344090 Rostov-on-Don, Russia
[f] Department of Physics, Faculty of Science, Al-Azhar University, Assiut 71542, Egypt
[g] Semiconductor Lab., Physics Department, Faculty of Education, Ain Shams University, Roxy, 11757 Cairo, Egypt
[h] Research Center for Advanced Materials Science (RCAMS), King Khalid University, P.O. Box 9004, Abha 61413, Saudi Arabia
[i] Center of Medical and Bio-Allied Health Sciences Research, Ajman University, Ajman P.O. Box 346, United Arab Emirates.

ARTICLE INFO

Keywords:
Sol-gel spin-coating
Thin films
Metal oxides
Doping
Dielectric properties

ABSTRACT

In the present investigation, a low-cost and high-operational sol-gel spin coating technique for preparing undoped and various Europium (Er)-doped CdO films of molar percentages of 1%, 5%, 10%, and 15% were considered. Using X-ray diffraction, the polycrystalline nature reveals two preferred orientations of (111) and (200). The mean crystallite size was evaluated and increased from 20.95 to 49.37 nm using the well-known Scherer's formula by increasing the Eu- dopant content. The atomic force microscopy images indicate a homogeneity of a granular distribution deteriorated with Eu-content. The root means square roughness value was evaluated and increased from 4.1 nm to 284 nm with Eu-doping. High transmission of approximately 80% in the visible region spectrum was recorded. The optical band gaps are increased from 2.2 to 2.46 eV from the undoped and various Eu-content %. A relationship between the Eu- content % for CdO films and the optical parameters was discussed to support the availability of the device for optoelectronic applications.

1. Introduction

Transparent conductive oxide (TCO) films have gained a lot of attention in recent years due to their high optical transmittance and low resistivity. Numerous research groups have used them since they have potential applications in renewable energy, gas sensors, telecommunication storage devices, liquid crystal displays, biotech, phototransistors and photodetector, health application, and optical heaters, various optoelectronic implementations [1–5]. Among them, due to its attractive applications in optoelectronic devices,

* Corresponding author.
E-mail addresses: alaafaragg@edu.asu.edu.eg, alaafaragg@gmail.com (A.A.M. Farag).

https://doi.org/10.1016/j.ijleo.2023.170830
Received 25 June 2022; Received in revised form 4 March 2023; Accepted 27 March 2023
Available online 28 March 2023

flat panel displays, and transparent electronic devices, cadmium oxide (CdO) is the most researched metal oxide [6]. CdO has also been designed to be used in gas sensors, thin-film resistors, and low-emissive windows, also, CdO has a highly remarkable electrical conductance n-type semiconductor [6,7].

The methodology adopted for enhancing the characteristics is doping to improve the optical and electrical characteristics of CdO films. These properties can be finely tuned by the addition of dopants [8,9]. Various authors have reported on the addition of several types of elements to improve the optical and electronic characteristics of CdO, doping of CdO with appropriate elements like Fe, Mn, Ni, Cu, Co, Al, In, Gd, Eu, Ce, Sm, and La [8,9]. Doping with various metallic ions may regulate the electrical and optical properties of CdO. The doping of CdO with metallic ions of a smaller ionic radius than that of Cd^{2+}, such as In, Sn, was experimentally identified. As explained by the Moss-Burstein (B-M) effect, Al, Sc, and Y enhance their electrical conduction and increase their optical energy gap [10–14]. Erdoğan et al. [15] investigated the effect of Lu doping on the physical, structural, and surface features of CdO film-based devices to improve their efficiency. Due to its ionic radius resemblance to cadmium oxide and matching with the number of oxidation states, the rare-earth element Europium (Eu) is an outstanding doping element for CdO structure [16]. Ganesh and AlFaify [17] have investigated the linear and nonlinear optical characteristics of sol-gel spin-coated Eu-doped CdO thin films with doping contents of 1%, 2.5%, 5.0%, and 10.0%. They found that the changing of the doping content increased the indirect energy bandgap from 2.52 to 2.69 eV in all of the investigated structures.

Many studies have examined the optoelectronic characteristics of CdO doped with a variety of ions, including indium, aluminum, gallium, and manganese [18–21]. When Eu^{2+} ions are replaced by Cd^{2+} ions in the CdO lattice, the concentration of electron conduction is enhanced, resulting in improved conductivity as discussed by Ravikumar et al. [22]. Shannon [23] has provided a list of ionic radii as well as the relationships among radii, coordination number, and valence. They also looked into issues including polyhedral distortion, partial occupancy of cation sites, covalence, and electron delocalization that could cause the radii sums to deviate from additivity.

Many different techniques have been used to prepare CdO films like sol-gel [24,25], chemical bath deposition (CBD) [23], magnetron sputtering [26], pulsed laser deposition [27], successive methods of ionic layer adsorption and reaction (SILAR) [27,28] and metal-organic chemical vapor deposition [29].

Because just a few researchers are thinking about developing and description of undoped and various Eu-doped CdO thin films formed using a low-cost approach, there is a need to understand these features, which have a significant impact on device performance. When Eu-doped CdO thin films are utilized in devices, such as solar cells, it is critical to present a detailed investigation of their structural and optical properties.

In the present work, Eu ions were used as a dopant with different concentrations for CdO(1%, 5%, 10%, and 15%). Eu ions can normally exist in two valency states, i.e., Eu^{2+} and Eu^{3+} as Eu^{3+} ions replace some Cd^{2+} ions in the crystalline structure of CdO [CdO: Eu]. The concentration of conduction electrons should be increased when Eu^{3+} ions replace some Cd^{2+} ions in the CdO crystalline structure [CdO: Eu], which leads to electrical conductivity improvement. Moreover, ion Eu^{3+} has a standard 6-ionic coordination radius of 0.0947 nm, slightly less than that of Cd^{2+}, 0.097 nm [30]. Accordingly, we attempted to incorporate Eu ions for Cd ions to verify the enhancement of the structural and optical properties. Another importance is to check how Eu- doping influences the optoelectronic properties of CdO. A few studies are accessible for Eu-doped CdO nanostructured films on the comprehensive measurements of linear and nonlinear optical parameters to date. Consequently, using Kramer's Kronig relations, it is worth examining the linear and nonlinear optical characteristics of Eu-doped CdO films prepared by utilizing low-cost sol-gel spin coating. Finally, this work will also look at how the Eu-dopant CdO thin film affects structural and optical properties in optoelectronics.

2. Experimental technique

2.1. Synthesis and Eu-doped CdO nanostructured films preparation

As starting materials, cadmium acetate, purchased from Sigma Aldrich with a purity of 99.9%, and Europium nitrate, purchased from Merk with a purity of 98.0% were used for preparing the undoped CdO and Eu-doped CdO films using a low-cost sol-gel spin coating method. cadmium acetate was firstly dissolved in 2 methoxy ethanol (0.5 M) and agitated for 1 h on a magnetic stirrer at 70 °C. As a stabilizer, monoethyl amine of 0.5 M was applied, and the continued stirring for 1 h. Europium nitrate is dissolved in the above solutions in a range of molar percentages of 1%, 5%, 10%, and 15% for Eu doping. The formulations prepared were then cooled to 25 °C and aged for 2 days (48 H).

The Fluorine-doped Tin Oxide (FTO) coated glass substrates (with a resistivity of FTO ranges from 7 to 15 ohm/sq. and thickness of 500 nm) were washed with water and isopropanol to extract unnecessary dust and impurities before the coating process began. After the cleaning process, the substrates were completely dried at 120 °C for 10 min to evaporate the undesirable solvent. At a fixed rpm of 1500 for 30 s, the solutions that were prepared were dropped on a cleaned substrate. The same procedure was performed ten times to achieve a homogeneous thickness, and all the coated films were annealed at 450 °C for 2 h in the air.

2.2. Characterization techniques

A Shimadzu Lab X-XRD-6000 with CuK_{α} (= 1.5406 Å) at 30 °C was used for the structural analysis of the undoped and Eu-doped CdO film.

The prepared films' topography characterization study was performed using atomic force microscopy through Nano-contact mode utilizing NT-MDT (Type Next, Russia). The grain size and the samples' surface roughness were achieved via the program attached to

this unit.

The spectrophotometer (JASCO-570) in the UV-Vis-NIR regions was used for measuring the transmittance, reflectance, and absorbance spectra of undoped and Eu-doped CdO thin film over the FTO substrates in the spectral range of 300–1000 nm at 30 °C.

3. Results and discussion

3.1. Structural and morphological analysis of Eu-doped CdO nanostructured films

The crystallinity properties of undoped and Eu-doped CdO of doping contents of 1,5%, 10%, and 15% were examined using XRD. The pattern of XRD is shown in Fig. 1(a) and (b). The figure shows that a preferred orientation is a characteristic peak at $2\theta = 33.1^{\circ}$ and 38.49° [31]. These peaks are consistent with the planes of (1 1 1) and (2 0 0) of CdO and match with the standard card (JCPDS card no. 01–073–2245). The results confirm that the samples are polycrystalline with a face-centered cubic structure [31,32]. No additional peaks or phases are observed for the Eu-doped samples, except for a small change in the intensity and the observed peaks' width due to the lattice contraction that affects the crystallite size. The introduction of Eu doping creates an internal microstrain in the host lattice. Microstructural disorder in the CdO lattice limits crystal growth. It broadens XRD diffraction peaks, thus reducing the diffraction peak's intensity by increasing the Eu –dopant content in the lattice of CdO. Moreover, the microstrain effect [33], which may be due to dislocation, inhomogeneity of lattice distortion, and grain surface relaxation [33], may result in the expansion of diffraction peak (111) of Eu-doped CdO thin films on increasing Eu concentration [33].

Using Scherrer's Eq., the XRD profile data were used to estimate the average crystallite size [34] (D) is determined as follows:

$$D = \frac{K\lambda}{\beta\cos\theta} \tag{1}$$

where β is the FWHM, $\lambda_{k\alpha} = 1.5418$ Å, K is the form factor (≈0.9). In Table 1, the average crystallite size, and D values are listed. The results indicate that D's values are slightly shifted with the Eu content change in CdO.

The average dislocation density (δ) is determined from the size of the crystallite using the following formula [34]:

$$\delta = \frac{1}{D^2} \tag{2}$$

Furthermore, the average microstrain (ε) can be calculated using the following [34]:

$$\varepsilon = \frac{\beta\cos\theta}{4} \tag{3}$$

The variation of D, δ, and ε of Eu: CdO films are inserted in Table 1, and from Fig. 2(d), it is notable that the dislocation density and micro-strain are enlarged for Eu doping concentration [35]. The values of D, δ, and ε of undoped and Eu-doped CdO thin films are shown in Fig. 2(a-c) and listed in Table 1. The results indicate that the dislocation density and micro-strain of the Eu doping concentration are increased due to the reduction of the mean crystallite size of the samples due to the incorporation of Eu [35].

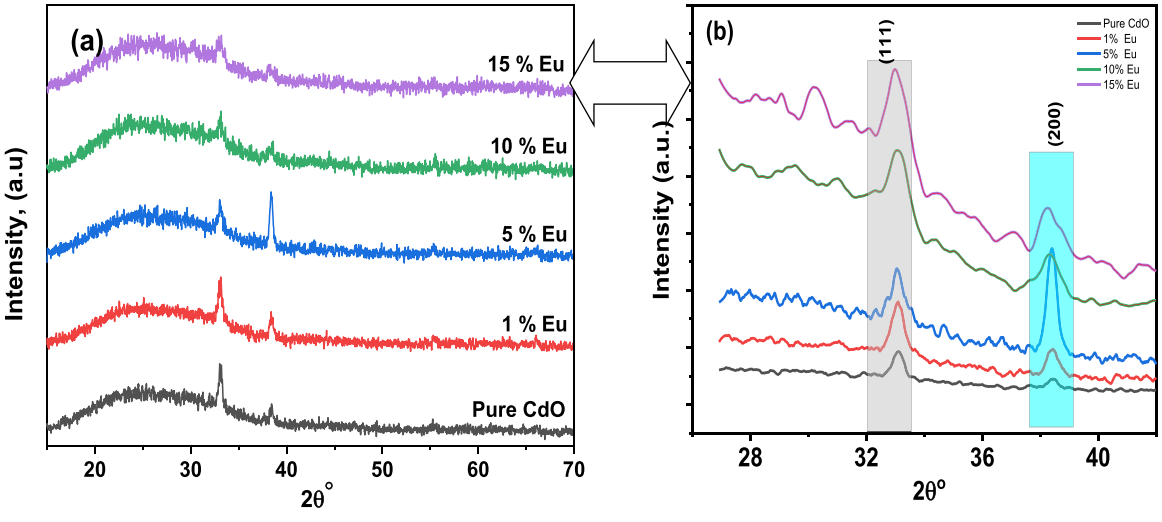

Fig. 1. (a) Full scaled XRD patterns and (b) Selected scale XRD patterns of the pure CdO and Eu-doped CdO thin films.

Table 1
Structural parameters of undoped and Eu-doped CdO thin films.

Sample Concentrations/ parameters	Peak position	FWHM	Mean crystallite Size, D (nm)	Lattice Strain, ε	Dislocation density, δ (nm^{-2})
Undoped CdO					
	33.1369	**0.3936**	**21.05799**	**0.33074**	**0.00226**
	38.4286	**0.3149**	**26.71622**	**0.22589**	**0.0014**
1% Eu-doped CdO	**33.0659**	**0.551**	**15.03975**	**0.46406**	**0.00442**
	38.3081	**0.4723**	**17.80618**	**0.33994**	**0.00315**
5% Eu-doped CdO	**33.0992**	**0.3149**	**26.31825**	**0.26493**	**0.00144**
	38.3923	**0.433**	**19.42727**	**0.31092**	**0.00265**
10% Eu-doped CdO	**33.1472**	**0.6298**	**13.16076**	**0.52905**	**0.00577**
	38.4569	**0.48**	**18.69781**	**0.22829**	**0.00286**
15% Eu-doped CdO					
	33.0199	**0.7872**	**10.52581**	**0.66396**	**0.00903**
	38.2317	**0.6298**	**13.35014**	**0.45428**	**0.00561**

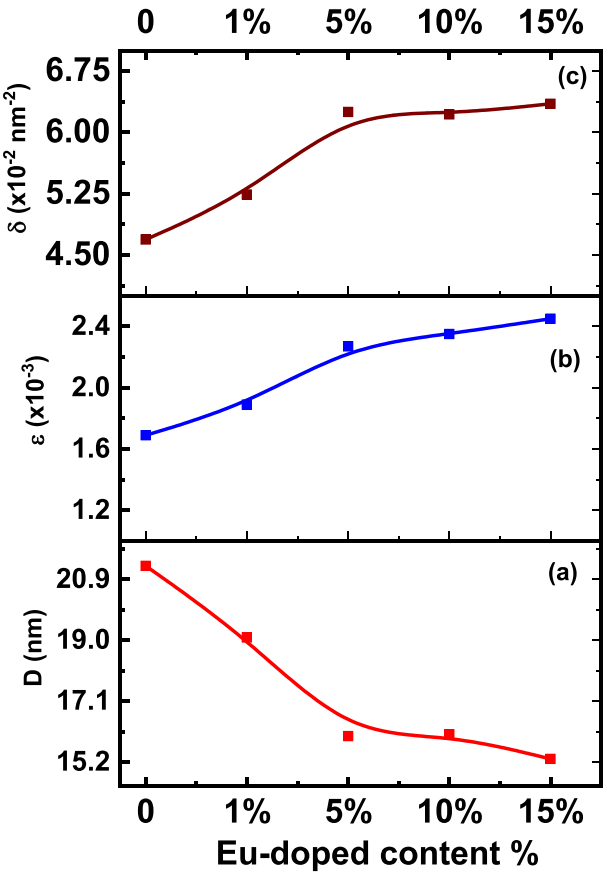

Fig. 2. (a) Mean crystallite size vs. Eu doped content, (b) Microstrain vs. Eu doped content, and (c) dislocation density vs. Eu doped content % CdO thin films for the (111) orientation.

3.2. AFM studies of Eu-doped CdO nanostructured films

Fig. 3 displays the images of the surface topography of the undoped and Eu-doped CdO films. A nearly uniform distribution is observed from the figures; all the films display fine spherical-shaped particles with different grain sizes depending on the Eu-content. Table 2 shows that the average grain size and the films' calculated roughness are measured using the P9 (IA-P9) program attached to the AFM instrument.

The results show that CdO's grain size tends to depend on the Eu element's doping content. Moreover, the results obtained from Fig. 3(a-e) and Table 2, in comparison with those published in the literature [22,36–44], indicate that the average grain size has a

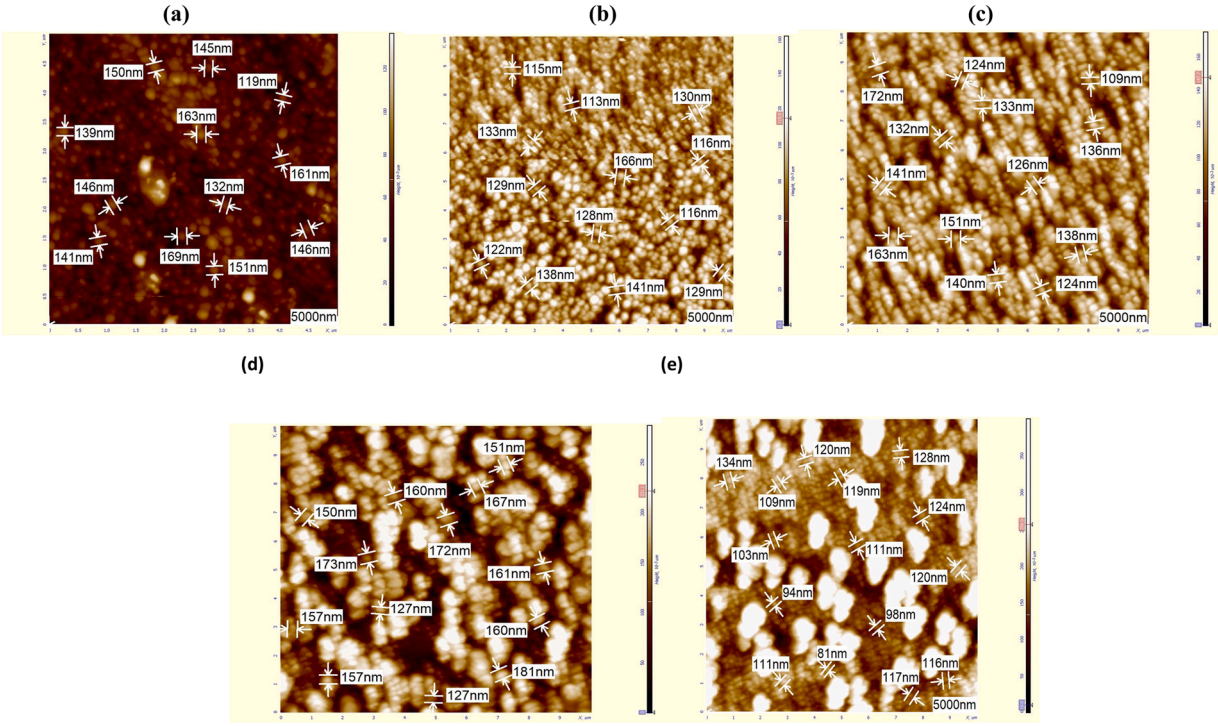

Fig. 3. AFM images of Eu-doped CdO thin films, (a) pure CdO. (b) 1% Eu-doped CdO,(c) 5% Eu-doped CdO,(d) 10%Eu-doped CdO, and (e) 15%Eu-doped CdO.

Table 2
The values of E_g for **Eu-CdO** thin films are incomparable to the previously reported data.

Compound	Grain size (nm)	Roughness (nm)	$E_g^{d\ allowed}$, eV	*T % at* $\lambda = 800$ *nm*	*n at* $\lambda = 600$ *nm*	*Ref.*
0.0% Eu-CdO	**146.8**	25.3	**2.2**	***73%***	***2.55***	**Present work**
1% Eu-CdO	**128.9**	33.6	**2.74**	**80%**	**2.25**	
5% Eu-CdO	**137.6**	39.5	**2.21**	**74%**	**1.9**	
10% Eu-CdO	**157.1**	45.2	**2.89**	**68%**	**1.8**	
15% Eu-CdO	**111.7**	33.9	**2.46**	**66%**	**2.2**	
Eu doped CdO(0–5%)	——	——	**2.42–2.33**	**62–30**	—	[22]
Sn -CdO films	——	**6.43–16.38**	**2.54–2.47**	**90.5–78**	**2.1–2.89**	[36]
Er- CdO/FTO films (0–10%)Er	**17.06–13.8**	**55.38–36.18**	**2.85–2.97**	**78–70**	**2.2**	[37]
F -CdO thin films(0–6%)F	**16.67–9.21**	**13.27–7.23**	**2.58–2.73**	**76–83**	**1.6–1.75**	[38]
Zn- CdO thin films(0–4%) Zn	**71.68–60.23**	**25.03–20.46**	**2.54–2.59**	**85–75**	**1.3–1.7**	[39]
CdO films.	——	———	**2.89–2.52**	**80–84**	**2.2**	[40]
Y:CdO films (0–4%) Y	———	———	**2.24–2.62**	**52–76**	**1.6–2.1**	[41]
Eu- CdO films(0–1.1%)Eu	——	———	**2.25–1.44**	**82–30**	——	[42]
Eu- and H-codoped CdO	———	———	**2.3–1.83**	**90–42**	——	[43]
Pt –CdO (0–2%)	**81.34–206.2**	**33.2–30.72**	**2.52–2.5**	**71–68**	**1.5–2.4**	[44]

reduction from 146.8 to 111.7 nm when the Eu-dopant concentration has risen from 1% to 15%. With rising Eu doping, the measured roughness is increased. Most probably, the surface roughness of the thin films increases with increasing grain size [45,46] but sometimes some opposite results are also reported [47]. Because the fabrication technique is also responsible for the various trend of surface roughness. The surface roughness is depending on the size, shape, and orientation of grains.

The film's roughness, which was raised from 25.3 to 33.9 nm, is compatible with the result obtained by Kathalingam et al. [33] for thin films of Sn-doped CdO. The reduction of the grain size of the films is due to the lattice distortion induced by the incorporation of Eu. Fig. 4 shows the three-dimensional-AFM and their related parameters, like particle size distribution and linear profile of the surface morphology. Furthermore, the results agree with those obtained by Ganesh et al. [34] for Erbium-doped CdO thin films and that obtained by Bagheri Khatibani et al. [35] for thin films with F-doped CdO as well as the results produced by Yahia et al. [36] for thin films with Zn-doped CdO. The obtained AFM results are consistent with XRD results and with those obtained by Ganesh et al. [37] for Erbium-doped CdO thin films and Bagheri Khatibani et al. [38] for F-doped CdO thin films, as well as those obtained by Yahia et al.

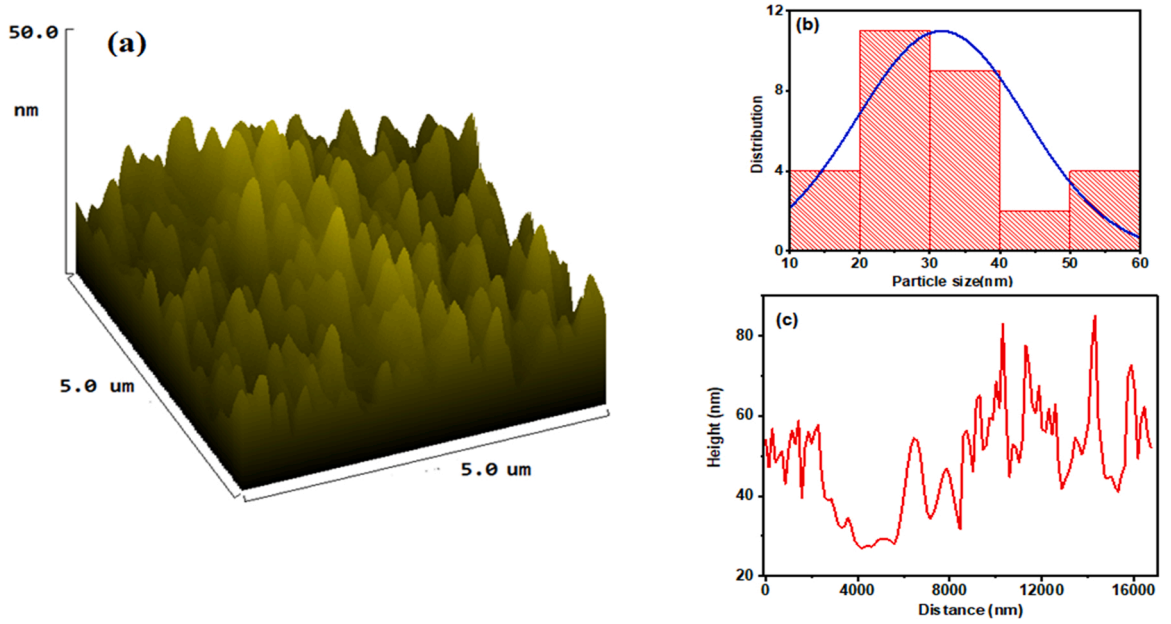

Fig. 4. (a) 3D-AFM images and (b) histogram distribution and (c) linear profile of the surface of undoped CdO thin films.

[36] for Zn-doped CdO thin films.

The obtained results show that the remarkable effect of Eu with different concentrations on the average grain size and roughness of the doped films enhances CdO thin films' structural properties, and consequently the optical and optoelectronic features.

3.3. Linear optical analysis of Eu-doped CdO nanostructured films

3.3.1. The theoretical background of Kramers-Kronig relations

The optical constants calculation is essential for the material application that controls its characteristics and performance. The Kramer-Kronig method is the preferred solution for precise optical constant calculations [37–39]. The Kramers-Kronig method was used to measure the optical constants for CdO thin films (n & k) as follows [48–50]:

$$N'(\omega) = n(\omega) + ik(\omega) \tag{4}$$

the refractive index n(ω) and extinction coefficient k(ω) of CdO thin films are determined as follows [48–50]:

$$n(\omega) = \frac{1 - R(\omega)}{1 + R(\omega) - 2\sqrt{R(\omega)}\cos\phi(\omega)} \tag{5}$$

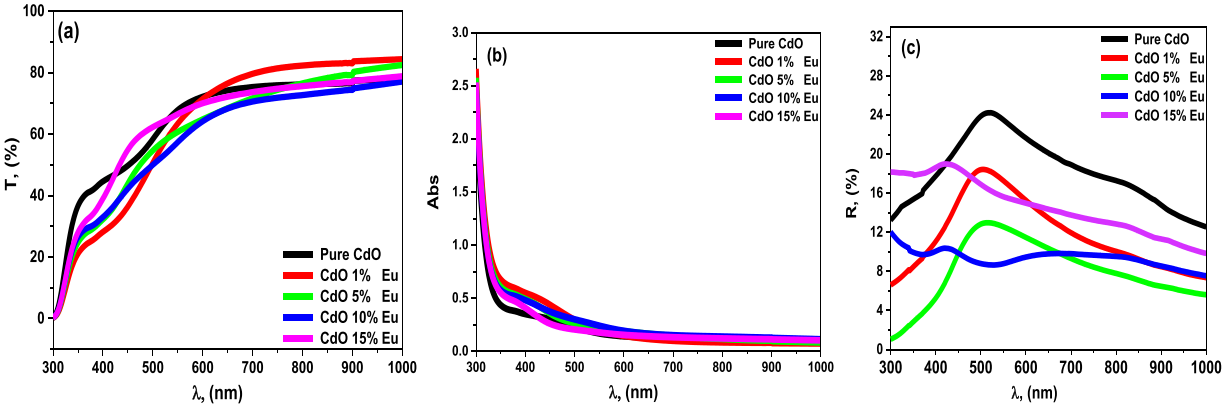

Fig. 5. (a) Spectral dependence of transmittance, T, (b) Spectral dependence of Absorbance, Abs., and (c) Spectral dependence of Reflectance, R of the pure CdO and Eu-doped CdO thin films.

$$k(\omega) = \frac{2\sqrt{R(\omega)}\sin\phi(\omega)}{1 + R(\omega) - 2\sqrt{R(\omega)}\cos\phi(\omega)} \quad (6)$$

Where ω is the angular frequency, and φ(ω) is the phase difference between incident and reflected radiation, which can be derived from the K-K dispersion relationship Fourier transform as described elsewhere [48–50].

Fig. 5(a, b, c) depicts the wavelength dependence of the T(λ), R(λ), and abs(λ) spectra of the undoped and Eu-doped CdO films between 300 and 1000 nm. The figure indicates that the transmittance increases in the beginning until the wavelength is almost 600 nm and then becomes independent of the incident light wavelength. The film transmission (T) varies in the range of 70 − 80% and slightly decreased with increasing Eu-doping. Similar behavior has been found with increasing doping concentrations published in the literature [22,36–44]. Such a transmittance reduction effect is also anticipated due to different surface plasmon excitation factors, improving grain size, and increasing roughness [51]. This decrease in transmittance may be due to an increase in absorption with increasing the Eu doping content in the lower region of the spectrum (i.e., UV region) [52]. The observed edge of transmittance spectra relates to the energy gap of the undoped and Eu-doped CdO. It depends on excitation energy from the valence band to the conduction band, which was previously explained for the metal oxide in detail [53,54]. The lower Eu concentration in the CdO lattice raises the semiconductor's optical band by increasing the electron density and allocating more photon energy to transfer from CB's valence due to the smaller grain size. The Burstein Moss shift [55] illuminates this widening effect in the band gap with doping. The reflectance spectra of the thin films of CdO and Eu-doped CdO, shown in Fig. 5(C), indicate that the CdO thin film reflectance range is affected by incorporating Eu doping. The reflectance spectrum of undoped-CdO thin films has been revealed to be higher than that of other doped Eu-CdO thin films.

The study of the absorption coefficient (α) is significant to predict any changes in the matrix's electronic band [53]. The spectra of optical absorption can be used to determine the indirect and direct transitions that possibly arise in the material bandgap [38]. It is known that the investigation of the absorption edge gives useful information regarding the bandgap. During the absorption process, the edge of absorption is specified. The absorption coefficient (α) was determined via the following relationship [52,53]:

$$\alpha = \frac{1}{d}\left(\frac{(1-R)^2}{2T} + \sqrt{\frac{(1-R)^4}{4T^2} + R^2}\right) \quad (7)$$

where d is the thickness of the films.

Tauc's relationship [56] can be used to calculate the direct band gaps, E_g of the undoped and Eu doped CdO films, using the absorption coefficient α as follows:

$$\alpha h\upsilon = A\left(h\upsilon - E_g\right)^m \quad (8)$$

where A is a constant, and m is another constant whose value is 1/2 for the allowed direct transition or 2 for the allowed indirect transition. Accordingly, the energy gap can be calculated from the extrapolation of the linear plot segment of $(\alpha h\upsilon)^2$ vs. hυ. Fig. 6 shows the plot of $(\alpha h\upsilon)^2$ vs. hυ of undoped and Eu-doped CdO thin film. With the intercept of the energy axis, the E_g values increase from 2.2 eV (undoped CdO) to 2.46 eV with an increase in the doping concentration of Eu in addition to some undulations. Such behavior in the bandgap can be viewed because of expanding the Burstein-Moss bandgap [55] and supported by various authors [57–59]. The Fermi level lies inside the conduction band for degenerate semiconductors like CdO, where its location depends on the free electrons' density. The excitation of the electrons from the top of the valence band to the bottom of the conduction band is correlated with

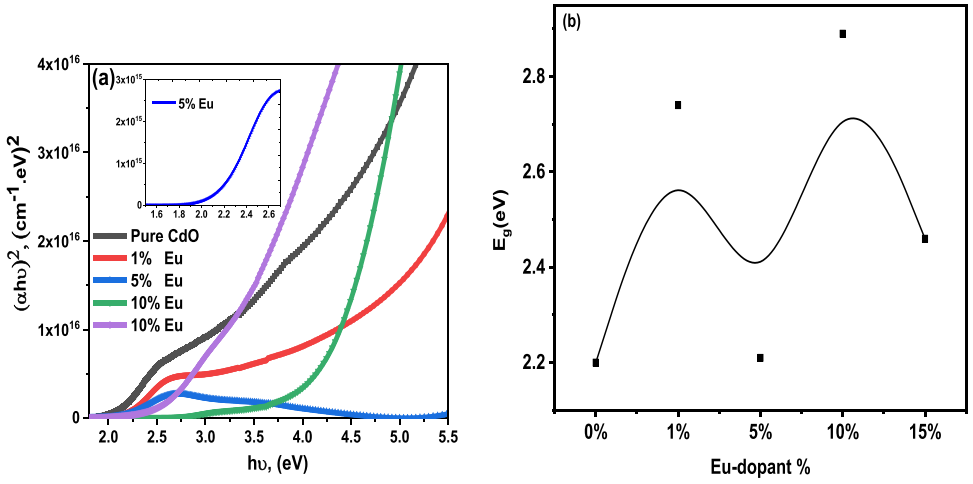

Fig. 6. Plot of $(\alpha h\upsilon)^2$ vs. $h\upsilon$ curves of the pure CdO and Eu-doped CdO thin films.

persistent optical band gaps. The likelihood of donor states may be increased in Eu: CdO thin film, and, at the same time, oxygen vacancies may be decreased. Consequently, because of the rise in the carrier density, the Fermi level's lifting into the degenerate semiconductor's conduction band provides an extension/broadening of the energy band due to the increase of Eu-doping content [59]. The measured energy gap of undoped and Eu-doped CdO thin film is comparable to previous reports on similar materials doped with Eu and other dopants [22,36–44] and listed in Table 2. The higher optical bandgap with doping was recorded by Ganesh et al. [37] for Er- CdO thin films from 2.85 to 2.97, while Ahmed et al. [41] recorded the change of bandgap from 2.24 to 2.62 eV for Y- doped CdO thin film. Furthermore, the same pattern was reported for thin F-CdO films by Khatibani et al. [40] and thin Zn-CdO films by Yahia et al. [39]. The widening of the optical bandgap can be attributed to the Burstein-Moss effect [60]. This could happen because of transition metal atom doping, which is one of the most effective techniques to increase the charge carrier density of conduction band states. As a result, when all states closer to the conduction band become occupied and the absorption edge shifts to higher energy, the optical band gap of a semiconductor rise [60].

For optical applications, the refractive and absorption indices are essential parameters and can offer information on the behavior of light, dispersion, and absorption properties of the investigated material. Therefore, the optical parameters of undoped CdO and Eu-doped CdO films should be addressed. Fig. 7(a) displays the refractive index's plot vs. wavelength of thin films of the undoped and Eu-doped CdO films using the K-K relations.

As depicted in Fig. 5(a), the refractive index plot consists of two regions known as abnormal and normal dispersion regions. In the anomalous dispersion field, the n values of the CdO and Eu-doped CdO thin films increase as λ increases. In comparison, in the typical dispersion area, the refractive index (n) values of the CdO and Eu-doped CdO thin films decline with increasing wavelength. The CdO thin film refractive index values also change with Eu doping, and the undoped CdO thin film refractive index is the highest value, while the 5% Eu-CdO thin film refractive index is the lowest value compared with those other films. The value of n for the undoped and Eu-CdO films is calculated at 600 nm and found to agree with those published for various doped CdO films [22,36–44] as listed in Table 2. The change in the value of k of undoped CdO and Eu-doped CdO thin films vs. wavelength is shown in Fig. 7(b). As the Eu doping concentration rose, the k-value of films decreased. At certain wavelength regions($\lambda > 800$ nm), the value of k of the undoped CdO is lower than the Eu-doped films.

The real part of the dielectric constant ε reflects the material's ability to store energy and is connected to polarization, while the imaginary part, ε_i is responsible for wave damping and energy dissipation.

The dielectric constant of a semiconductor is widely used in the manufacture of capacitors and controlling the stored energy in the electric field between the plates, as well as filtering out noise from signals as part of a resonant circuit. The capacitor can store more charge in a given field if the dielectric constant is higher. High electrical resistivity and low dielectric loss are the most desirable features for some applications of dielectrics rely, depending on their electrically insulating capabilities rather than their capacity to retain a charge. Insulation for wires, cables, and other such items is the most obvious application, but it also has applications in sensor devices. The dielectric constant is typically measured under alternating current at a specific applied frequency, which is referred to as the static dielectric constant. This is frequently substantially different from the dielectric constant calculated from the refractive index at a visible light frequency of 10^{15} Hz.

The real part of the dielectric constant, ε and the imaginary part, ε_i of the dielectric constants of undoped and Eu-CdO films are calculated by the following equations [39]:

$$\varepsilon = n^2 - k^2 \tag{9}$$

$$\varepsilon_i = 2nk \tag{10}$$

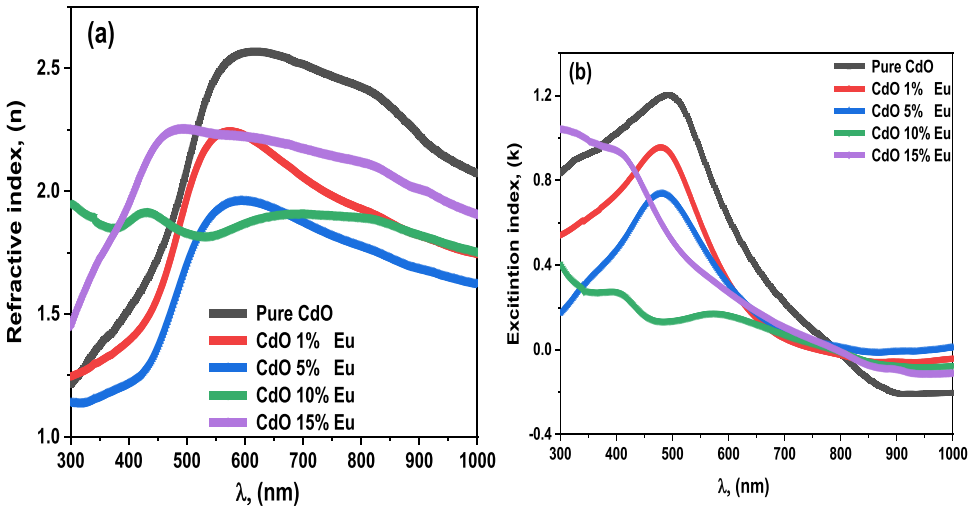

Fig. 7. (a) Plot of refractive index, n vs. λ, and (b) Extinction coefficient, k vs. λ of the pure CdO and Eu doped CdO thin films.

Fig. 8(a,b) shows the real dielectric constant (ε_1) and the imaginary part (ε_2) of the undoped and Eu-doped CdO films. In the near UV–visible region, the ε_1 values ranged from 2.0 to 6.5, and ε_2 increased from 0.4 to 5.2. Characteristic peaks are observed for the measured ε_1 for all the films, with the undoped CdO film's highest intensity.

The real optical conductivity, σ, and the imaginary optical conductivity, σ_i are related to the dielectric constants and can be used to analyze the optical properties of the undoped CdO and Eu doped CdO thin films as follows [39,40]:

$$\sigma_1 = \omega\varepsilon_o\varepsilon_2 \;\&\; \sigma_2 = \omega\varepsilon_o\varepsilon_1 \tag{11}$$

Optical conductivity is the extension of electrical transport to high (optical) frequencies. It is a contact-free quantitative measurement, mostly sensitive to charged responses. The real and imaginary parts of the undoped CdO and Eu-doped CdO thin films' optical conductivity are shown in Fig. 9(a,b), respectively. As seen from the figure, the real part $\sigma(\omega)$and the imaginary part$\sigma_i(\omega)$.The optical conductivity displays a characteristic peak shifted under the influence of Eu doping material with wavelengths up to around 600 nm. Due to the maximum value of the real dielectric at this wavelength, undoped CdO films have a higher intensity.

The other important parameter is the high-frequency electrical conductivity which can be estimated based on the optical conductivity stated by various authors as in the following relation [61,62].

$$\sigma_e = \frac{2n\omega}{\alpha c}\sigma_{opt} \tag{12}$$

The wavelength dependency of σ_e is shown in Fig. 10 for the undoped CdO and Eu-doped CdO thin films. With increasing wavelength, σ_e values rise for all the studied films. Compared to the other Eu-doped CdO films, the undoped CdO films showed a higher electric conductivity at higher wavelengths ($\lambda \geq 500$ nm). The rise in the electrical conductivity at long wavelengths could be due to the high absorption coefficient of the studied thin films [61,62].

3.4. Non-linear optical properties of undoped and Eu-doped CdO nanostructured films

Due to their applications in storage, display, and optical instruments, the measurement of thin films' nonlinear optical properties takes a lot of significance. In addition to providing complete details about their practical use, these properties often provide information about device implementations in the specific optical spectrum.

Nonlinear optics is a field of optics that focuses on the analysis of light in nonlinear media or media in which the polarization density P responds nonlinearly to the light's electric field E. Only very high light intensities (values of atomic electric fields, generally 10^8 V/m) such as those given by lasers produce non-linearity. The vacuum is projected to become nonlinear over the Schwinger limit. The superposition principle is no longer valid in nonlinear optics. The nonlinear refractive index, n_2, depends primarily on the incident light intensity. The polarization and the electric field are no longer proportional when the deposited film is exposed to the strong electric field's incident light. The difference in polarizability must be elongated by the terms proportional to the square electric field [63]. Different nonlinear optical parameters can be used for the calculation of the Eu effect on undoped CdO using polarizability (P) and nonlinear polarizability using the following relationships [63–65].

$$p = \chi^{(1)}E + P_{NL} \tag{13}$$

where

$$P_{NL} = \chi^{(2)}E^2 + \chi^{(3)}E^3 \tag{14}$$

Where $\chi^{(1)}$ is linear optical susceptibility, where P is polarizability, $\chi^{(2)}$ is the second-order non-linear optical susceptibility, and $\chi^{(3)}$ is third-order non-linear optical susceptibility. The linear optical susceptibility $\chi^{(1)}$ for a medium can be obtained from the following equation [64]:

$$\chi^{(1)} = \left(n^2 - 1\right)/4\pi \tag{15}$$

Based on linear refractive index $n_0(\lambda)$, the relation between third-order non-linear optical susceptibility $\chi^{(3)}$ and linear optical susceptibility $\chi^{(1)}$ can be expressed as follows:

$$\chi^{(3)} = \frac{A}{(4\pi)^4}\left(n_0^2 - 1\right)^4 \tag{16}$$

For various kinds of materials, the value of the constant (A) value equals 1.7×10^{-10} (for $\chi^{(3)}$ in esu). In addition, the non-linear refractive index can be described as:

$$n_2 = \frac{12\pi\chi^{(3)}}{n_o} \tag{17}$$

As a function of wavelength, the behavior of linear, third-order nonlinear susceptibility and nonlinear refractive index is shown in Fig. 11 (a-c). Accordingly, it is recognized that all parameters behave in the same manner.

The $\chi^{(1)}$ values are found to be in the 0.025–0.45 range, third-order susceptibilities 6.5×10^{-12} esu to 1.9×10^{-12} esu, and nonlinear refractive index values are in the range of 0.5×10^{-12} esu to 7×10^{-12} esu. The $\chi^{(1)}$ and $\chi^{(3}$and n_2 values are tabulated in

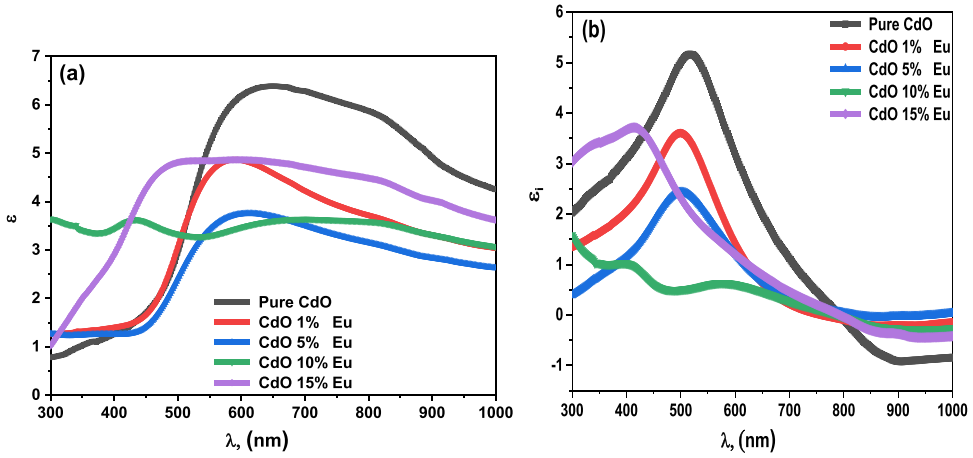

Fig. 8. (a) Plot of real dielectric constant, ε vs. λ, and (b) Plot of imaginary dielectric constant (ε_1) of the pure and Eu-doped thin films.

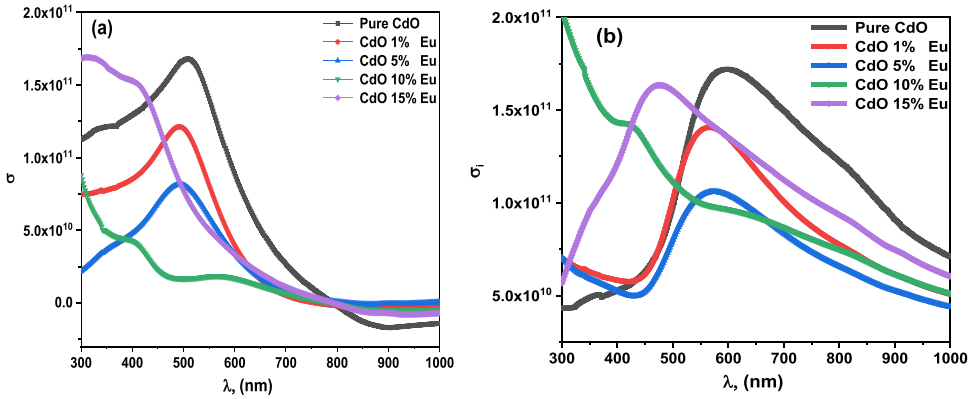

Fig. 9. a) Plot of real optical conductivity, σ vs. λ, and (b) Plot of imaginary optical conductivity, σ_I of the pure and Eu-doped thin films.

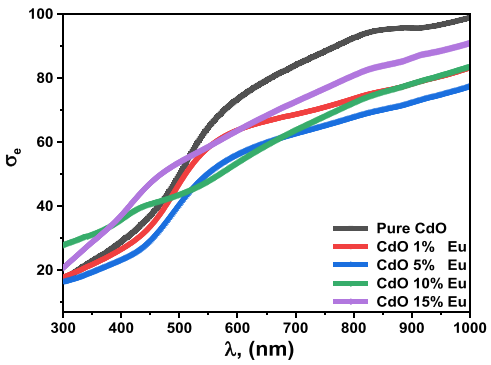

Fig. 10. Plot of the electrical conductivity, σ_e vs. λ of the pure and Eu doped CdO thin films.

Table 3, compared with those published in the literature [37–39]. There are an increase and a decrease in the nonlinear optical values by doping Eu, which presumably improves/decreases the optical nonlinearity of the CdO films showing Eu at the CdO films. The observed optical nonlinearity reveals the presence of defects in the Eu: CdO films; furthermore, nonlinearity is changed with varying the wavelength and dopant owing to variation in particle size of all the films [66]. Compared to the previously recorded values for Er-doped CdO by Ganesh et al. [34], the existing optical nonlinearities of undoped and Eu-doped CdO films are lower, which is between 2 and 7. The recorded optical nonlinearities ofEu -doped CdO films are lower compared to the previously reported values for Er-doped CdO by Ganesh et al. [37], Yahia et al. [39] for Zn- CdO thin films reported, and Khatibani et al. [38] for F- CdO thin films.

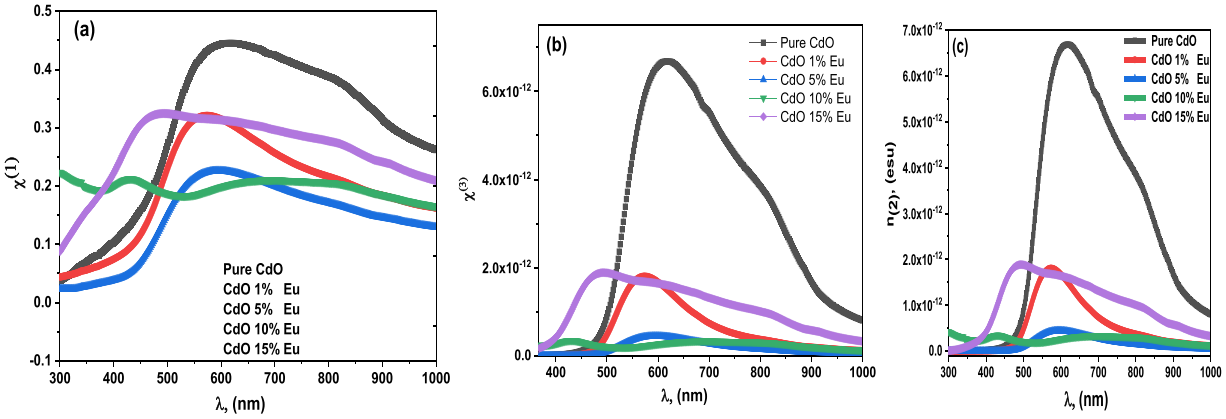

Fig. 11. (a) Plot of $\chi^{(1)}$ vs. λ, (b) Plot of $\chi^{(3)}$ vs. λ, and (c) Plot of n_2 vs. λ of the pure CdO and Eu-doped CdO thin films.

Table 3
The values of $\chi^{(1)}$ and $\chi^{(3)}$ and n_2 for **Eu-CdO** thin films are incomparable to the previously reported data.

Samples	Technique	$\chi^{(1)}$ esu	$\chi^{(3)}$ *esu at*	n_2	Ref.
0.0% Eu-CdO	sol-gel	0.445	6.6×10^{-12}	6.7×10^{-12}	Present work
1% Eu-CdO		0.32	1.8×10^{-12}	1.7×10^{-12}	
5% Eu-CdO		0.27	0.5×10^{-12}	0.49×10^{-12}	
10% Eu-CdO		0.19	0.4×10^{-12}	0.22×10^{-12}	
15% Eu-CdO		0.31	1.9×10^{-12}	1.69×10^{-12}	
Er-doped CdO thin films on FTO (1–10) Er	sol-gel	2–7	1.6×10^{-13} - 5.41×10^{-13}	1.39×10^{-12} - 8.1×10^{-11}	[37]
F- CdO (0–6) %	**spray pyrolysis**	–	0.8×10^{-13} - 5×10^{-13}	——	[38]
Zn- CdO thin films (1–4) wt%	sol-gel	0.02 –0.13	1×10^{-14} to 5.2×10^{-14}	1×10^{-13} - 1.4×10^{-12}	[39]

4. Conclusion

In conclusion, the high-quality and low-dimensional nanostructured CdO films with varied Eu-dopings have been achieved using the sol-gel spin coating approach. The results of XRD studies confirm the polycrystalline nature of films and confirm the low-dimensional formation of nanocrystalline films with mean crystallite sizes from 20 nm to about 50 nm depending on the Eu-dopant %. Moreover, the lattice strain and the dislocation density were reduced due to enhancing the films' crystallinity. The AFM images have verified the nanoparticles' distribution with a mean grain size of 146.8–111.7 nm and roughness values of 25.3–33.9 nm for different Eu doping %. Due to various surface plasmon excitation factors, improving grain size, and increasing roughness, the film transmission varies between 70% and 80% and slightly decreases with increasing Eu-doping. The Kramer-Kronig method was used to calculate the optical constants. The optical band gap is found to be direct allowed with values influenced by Eu- doping content and ranged between 2.2 and 2.46 eV. The indices of the dispersion parameters were also calculated and confirmed the Eu doping content's role in controlling their variable optical applications' values. The measured optical nonlinearity confirms the occurrence of defects in the Eu: CdO films; additionally, nonlinearity varies with wavelength and dopant due to particle changes in size in all films. The optical properties results ensure that the CdO's Eu-dopant films are an essential candidate for the use of optoelectronic equipment. The effect of Eu on cadmium oxide has been covered in this work, but a larger study will be undertaken in the future to control crystal sizes and increase the effect with more precise ratios, as well as the effect of sensitivity of Eu-doped CdO heterojunction diodes under the influence of light.

Declaration of Competing Interest

The authors declare that they have no known competing financial interests or personal relationships that could have appeared to influence the work reported in this paper.

Data availability

The data that has been used is confidential.

Acknowledgment

Many thanks to Ain Shams University. Thanks and gratitude to The Research Center for Advanced Materials Science (RCAMS)" at King Khalid University, Saudi Arabia, for funding this work under the grant number RCAMS/KKU/017-22.

References

[1] B. Ravi Kumar, K. Hari Prasad, K. Kasirajan, M. Karunakaranc, V. Ganeshd YugandharBitlae, S. AlFaify, I.S. Yahia, Enhancing the properties of CdO thin films by co-doping with Mn and Fe for photodetector applications, Sens. Actuators A Phys. 319 (2021), 112544.
[2] K. Kasirajan, A. Nancy, Anna Anasthasiya, Omar M. Aldossary, Mohd Ubaidullah, M. Karunakaran, Structural, morphological, optical, and enhanced photodetection activities of CdO films: an effect of Mn doping, Sens. Actuators A Phys. 319 (2021), 112531.
[3] Serif Ruzgar, Yasemin Caglar, Ozgur Polat, Dinara Sobola, Mujdat Caglar, The tuning of electrical performance of Au/(CuO: La)/n-Si photodiode with La doping, Surf. Interfaces 21 (2020), 100750.
[4] W. Hu, H. Cong, W. Huang, Y. Huang, L. Chen, A. Pan, C. Xue, Germanium/perovskite heterostructure for high-performance and broadband photodetector from visible to infrared telecommunication band, Light Sci. Appl. 8 (2019) 1–10.
[5] B. Sürücü, H.H. Güllü, M. Terlemezoglu, D.E. Yildiz, M. Parlak, Determination of current transport characteristics in Au-Cu/CuO/n-Si Schottky diodes, Phys. B Condens. Matter 570 (2019) 246–253.
[6] S. AlFaify, V. Ganesha, L. Haritha, Mohd Shkir, An effect of La doping on physical properties of CdO films facilely casted by spin coater for optoelectronic applications, Physica B 562 (2019) 135–140.
[7] V. Ganesh, L. Haritha, H. Elhosiny Ali, Yasmin Khairy, H.H. Hegazy, V. Butova, Alexander V. Soldatov, H. Algarni, H.Y. Zahrana, I.S. Yahia, The detailed calculations of optical properties of indium-doped CdO nanostructured films using Kramers-Kronig relations, J. Non-Cryst. Solids 552 (2021), 120454.
[8] E. Gürbüz, R. Aydin, B. Şahin, A study of the influences of transition metal (Mn, Ni) co-doping on the morphological, structural, and optical properties of nanostructured CdO films, J. Mater. Sci. Mater. Electron. 29 (3) (2018) 1823–1831.
[9] S. AlFaify, V. Ganesh, L. Harith, Mohd Shkir, An effect of La doping on physical properties of CdO films facilely casted by spin coater for optoelectronic applications, Physica B562 (2019) 135–140.
[10] E. Burstein, Anomalous optical absorption limit in InSb, Phys. Rev. 93 (1954) 632–633.
[11] T.S. Moss, The interpretation of the properties of indium antimonide, Proc. Phys. Soc. Lond. B 67 (1954) 775–782.
[12] A.J. Freeman, K.R. Poeppelmeier, T.O. Mason, R.P.H. Chang, T.J. Marks, Chemical and thin-film strategies for new transparent conducting oxides, Mater. Res. Soc. Bull. 25 (2000) 45–51.
[13] R. Maity, K.K. Chattopadhyay, Synthesis, and characterization of aluminum-doped CdO thin films by sol-gel process, Sol. Energy Mater. Sol. Cells 90 (2006) 597–606.
[14] S. Shu, Y. Yang, J.E. Medvedova, J.R. Ireland, A.W. Metz, J. Ni, C.R. Kannewurf, A.J. Freeman, T.J. Tobin, Dopant ion size and electronic structure effects on transparent conducting oxides. Sc-doped CdO thin films grown by MOCVD, J. Am. Chem. Soc. 126 (2004) 13787.
[15] E. Erdoğan, G. Turgut, M. Yilmaz, Sol–gel spin coating derived cadmium oxide semiconductor thin films: effect of lutetium contribution, Optik 240 (2021), 166819.
[16] M. Ravikumar, V. Ganeshef Mohd Shkir, R. Chandramohan, K. Deva Arun Kumar, S. Valanarasu, A. Kathalingam, S. AlFaify, Fabrication of Eu doped CdO [Al/Eu-nCdO/p-Si/Al] photodiodes by perfume atomizer based spray technique for optoelectronic applications, J. Mol. Struct. 1160 (2018) 311–318.
[17] V. Ganesh, S. AlFaify, Linear and nonlinear optical properties of sol-gel spin-coated erbium- doped CdO thin films, Phys. B Condens. Matter 570 (2019) 58–65.
[18] R. Gupta, K. Ghosh, R. Patel, S. Mishra, P. Kahol, Structural, optical and electrical properties of in doped CdO thin films for optoelectronic applications, Mater. Lett. 62 (2008) 3373–3375.
[19] I. Yahia, G. Salem, M.A. El-sadek, F. Yakuphanoglu, Optical properties of Al-CdO nano-clusters thin films, Superlattice Microst. 64 (2013) 178–184.
[20] R. Deokate, S. Salunkhe, G. Agawane, B. Pawar, S. Pawar, K. Rajpure, A. Moholkar, J. Kim, Structural, optical and electrical properties of chemically sprayed nanosized gallium doped CdO thin films, J. Alloy. Compd. 496 (2010) 357–363.
[21] K. Sankarasubramanian, P. Soundarrajan, T. Logu, S. Kiruthika, K. Sethuraman, R.R. Babu, K, RamamurthiInfluence of Mn doping on structural, optical and electrical properties of CdO thin films prepared by cost effective spray pyrolysis method, Mater. Sci. Semicond. Process. 26 (2014) 346–353.
[22] M. Ravikumar, V. Ganesh, Mohd Shkir, R. Chandramohan, K. Dev aArun Kumar, S. ValanarasucA, KathalingamdS. AlFaify, Fabrication of Eu doped CdO [Al/Eu-nCdO/p-Si/Al] photodiodes by perfume atomizer based spray technique for opto-electronic applications, J. Mol. Struct. 1160 (2018) 311–318.
[23] R.D. Shannon, Revised Effective, Ionic radii and systematic studies interatomic distances in halides and chalcogenides, Acta Cryst. A32 (1976) 751–767.
[24] J.S. Cruz, G.T. Delgado, R.C. Perez, et al., Dependence of electrical and optical properties of sol-gel prepared undoped cadmium oxide thin films on annealing temperature, Thin Solid Films 493 (2005) 83–87.
[25] L.R. de Leon-Gutierrez, J.J. Cayente-Romero, J.M. Peza-Tapia, E. Barrera-Calva, J.C. Martınez-Flores, M. Ortega-Lopez, Some physical properties of Sn-doped CdO thin films prepared by chemical bath deposition, Mater. Lett. 60 (2006) 3866–3870.
[26] T.K. Subramanyam, S. Uthanna, B.S. Naidu, Preparation and characterization of CdO films deposited by dc magnetron reactive sputtering, Mater. Lett. 35 (1998) 214–220.
[27] M. Yan, M. Lane, C.R. Kannewurf, R.P.H. Chang, highly conductive epitaxial Cdo thin films prepared by pulsed laser deposition, Appl. Phys. Lett. 78 (2001) 2342–2344.
[28] R.R. Salunkhe, C.D. Lokhande, Effect of film thickness on liquefied petroleum gas (LPG) sensing properties of SILAR deposited CdO thin films, Sens. Actuators B 129 (2008) 345–351.
[29] B.ünyamin Fahin, Physical properties of nanostructured CdO films from alkaline baths containing saccharin as additive, Sci. World J. (2013), 172052.
[30] X. Liu, C. Li, S. Han, J. Han, C. Zhou, Synthesis and electronic transport studies of CdO nanoneedles, Appl. Phys. Lett. 82 (2003) 1950–1952.
[31] A.A. Dakhel, Bandgap narrowing in CdO doped with europium, Opt. Mater. 31 (2009) 691–695.
[32] N. Anitha, I. Anitha, L. Kulandaisamy Amalraj, Effect of substrates on the structural, morphological, and optical properties of sprayed CdO thin films using a nebulizer, J. Sol Gel Sci. Technol. 86 (2018) 580–589.
[33] N. Gonçalves, J. Carvalho, Z. Lima, J. Sasaki, Size–strain study of NiO nanoparticles by X-ray powder diffraction line broadening, Mater. Lett. 72 (2012) 36–38.
[34] A.M.S. Arulanantham, S. Valanarasu, K. Jeyadheepan, A. Kathalingam, Effect of thermal annealing on nebulizer spray deposited tin sulfide thin films and their application in a transparent oxide/CdS/SnS heterostructure, Thin Solid Films 666 (2018) 85–93.
[35] G. Turgut, G. Aksoy, D. İskenderoğlu, U. Turgut, S. Duman, The effect of Eu-loading on some physical features of CdO, Ceram. Int. 44 (2018) 3921–3928.
[36] A. Kathalingam, K. Kesavan, Abu ul Hassan Sarwar Rana, Joonhyeon Jeon, Hyun-Seok Kim, Analysis of Sn concentration effect on morphological, optical, electrical and photonic properties of spray-coated Sn-doped CdO thin films, Coatings 8 (2018) 167–174.
[37] V. Ganesh, S. AlFaify, Linear and nonlinear optical properties of sol-gel spin-coated erbium-doped CdO thin films, Physica B 570 (2019) 58–65.
[38] A. Bagheri Khatibani, Z.A. Hallaj, S.M. Rozati, Some physical properties of CdO:F thin films prepared by spray pyrolysis, Eur. Phys. J. 130 (2015) 254–260.
[39] I.S. Yahia, G.F. Salem, Javed Iqbal, F. Yakuphanoglu, Linear and nonlinear optical discussions of nanostructured Zn-doped CdO thin films, Physica B 511 (2017) 54–60.
[40] A. Abdolahzadeh Ziabari, F.E. Ghodsi, Optical and structural studies of sol-gel deposited nanostructured CdO thin films: annealing effect, Acta Phys. Pol. A 120 (2011) 536–540.
[41] S. Ahmed, M.S.I. Sarker, M.M. Rahman, M. Kamruzzaman, M.K.R. Khan, Effect of yttrium(Y) on structural, morphological, and transport properties of CdO thin films prepared by spray pyrolysis technique, Heliyon 4 (2018) e 00740.

[42] A.A. Dakhel, Bandgap narrowing in CdO doped with europium, Opt. Mater. 31 (2009) 691–695.
[43] A.A. Dakhel, Optoelectronic properties of Eu- and H-codoped CdO films, Curr. Appl. Phys. 11 (2011) 11–15.
[44] Z. Serbetci, B. Gunduz, A.A. Al-Ghamdi, F. Al-Hazmic, K. Ark, F. El-Tantawy, F. Yakuphanoglu, W.A. Farooq, Determination of optical constants of nanocluster CdO thin films deposited by sol-gel technique, Acta Phys. Pol. A 126 (2014) 798–807.
[45] Ahmet Tumbul, Improving grain size and surface roughness of chemically derived Cu_2CoSnS_4 (CCTS) solar absorber material by controlling of Cu/Co ratios, Ceram. Int. 46 (2020) 289–296.
[46] Aatif Ijaz, L.ászló Ferenc Kiss, A. Levent Demirel, Lajos K.ároly Varga, Annamária Mikó, Uning grain size, morphology, hardness and magnetic property of electrodeposited nickel with a single multifunctional additive, Mater. Chem. Phys. 267 (2021), 124681.
[47] Yuanhao Chen, Li Gou, Friction and wear behavior of diamond film with adjustable grain size against silicon carbide in different tribological tests, Diam. Relat. Mater. 129 (2022), 109377.
[48] E. Pakizeh, E. Pakizeh, Optical response and structural properties of Fe-doped Pb ($Zr_{0.52}$ $Ti_{0.48}$) O_3 nanopowders, J. Mater. Sci. 31 (2020) 4872–4881.
[49] F. Behzadi, E. Saievar-Iranizad, E. Pakizeh, Optical study on single-layer photoluminescent graphene oxide nanosheets through a simple and green hydrothermal method, J. Photochem. Photobiol. A 364 (2018) 595–601.
[50] A.M. Aboraia, A.A.A. Darwish, V. Polyakov, E. Erofeeva, V. Butova, Heba Y. Zahran, Alaa F. Abd El-Rehim, Hamed Algarni, I.S. Yahia, Alexander V. Soldatov, Structural characterization and optical properties of zeolitic imidazolate frameworks (ZIF-8) for solid-state electronics applications, Opt. Mater. 100 (2020), 109648.
[51] X. Yang, P. Gao, Z. Yang, J. Zhu, F. Huang, J. Ye, Optimizing ultrathin Ag films for high performance oxide-metal-oxide flexible transparent electrodes through surface energy modulation and template-stripping procedures, Sci. Rep. 7 (2017) 44576–44585.
[52] M. Shibata, H. Tokuya, S. Yamamoto, T. Saimei, T. Kato, T. Fukura, High-resistance ZrN thin film resistor for small and low-cost MMIC switch, Future of Electron Devices, Kansai (IMFEDK), IEEE International Meeting for IEEE (2012) 1–2.
[53] M. Arif, M. Shkir, V. Ganesh, A. Singh, H. Algarni, S. AlFaify, A significant effect of Ce-doping on key characteristics of NiO thin films for optoelectronics facilely fabricated by spin coater, Superlattice Microstruct. 129 (2019) 230–239.
[54] K. Ukoba, A. Eloka-Eboka, F. Inambao, Review of nanostructured NiO thin film deposition using the spray pyrolysis technique, Renew. Sustain. Energy Rev. 82 (2018) 2900–2915.
[55] E. Andrade, M. Miki-Yoshida, Growth, structure, and optical characterization of high-quality ZnO thin films obtained by spray pyrolysis, Thin Solid Films 350 (1999) 192–202.
[56] J. Tauc, R. Grigorovici, A. Vancu, Optical Properties and Electronic Structure of Amorphous Germanium, Phys. Status Solidi 15 (1966) 627–637.
[57] E. Erdoğan, G. Turgut, M. Yilmaz, Sol–gel spin coating derived cadmium oxide semiconductor thin films: effect of lutetium contribution, Optik 240 (2021), 166819.
[58] E. Erdogan, M. Yilmaz, S. Aydogan, G. Turgut, Investigation of neodymium rare earth element doping in spray-coated zinc oxide thin films, J. Mater. Sci. Mater. Electron 32 (2021) 1379–1391.
[59] Mohd Shkir, Mohd Arif, V. Ganesh, Arun Singh, H. Algarni, I.S. Yahia, S. AlFaify, An effect of Fe on physical properties of nanostructured NiO thin films for nonlinear optoelectronic applications, Appl. Phys. A 126 (2020) 119–136.
[60] Soniya Gahlawat, Jaspreet Singh, Ashok Kumar Yadav, Pravin P. Ingole, Exploring Burstein–Moss type effects in nickel doped hematite dendrite nanostructures for enhanced photo-electrochemical water splitting, Phys. Chem. Chem. Phys. 21 (2019) 20463–20477.
[61] A. Kamal Aly, Comment on the relationship between electrical and optical conductivity used in several recent papers published in the journal of materials science: Materials in Electronics, J. Mater. Sci. Mater. Electron 33 (2022) 889–2898.
[62] Hosam M. Gomaa, H.A. Saudi, I.S. Yahia, H.Y. Zahran, Extraction of the terahertz parameters from the UV–Vis optical conductivity of some $(NaB)_2O_4$ glasses doped with cerium oxide: a novel correlation between electrical & optical conductivities, J. Mater. Sci. Mater. Electron 33 (2022) 12397-12407.
[63] I.S. Yahia, G.F. Salem, Javed Iqbal, F. Yakuphanoglu, Linear and nonlinear optical discussions of nanostructured Zn-doped CdO thin films, Physica B 511 (2017) 54–60.
[64] P.M. Verghese, D.R. Clarke, Piezoelectric contributions to the electrical behavior of ZnO varistors, J. Appl. Phys. 87 (2000) 4430–4438.
[65] A. Jilani, Ms Abdel-Wahab, A.A. Al-Ghamdi, A. Sadik Dahlan, I. Yahia, Nonlinear optical parameters of nanocrystalline AZO thin film measured at different substrate temperatures, Phys. B Phys. 481 (2015) 97–103.
[66] Mohd Shkira, I.M. Ashraf, Kamlesh V. Chandekard, I.S.Yahia Aslam Khane, H. Algarni, S. AlFaify, A significant enhancement in visible-light photodetection properties of chemical spray pyrolysis fabricated CdS thin films by novel Eu doping concentrations, Actuators A Phys. 301 (2020), 111749.